Breakup of a Transient Wetting Layer in Polymer Blend Thin Films: Unification with 1D Phase Equilibria

Sam Coveney and Nigel Clarke
Department of Physics and Astronomy, University of Sheffield, Hicks Building, Hounsfield Road, Sheffield S3 7RH, United Kingdom
(Received 3 July 2013; published 20 September 2013)

We show that lateral phase separation in polymer blend thin films can proceed via the formation of a transient wetting layer which breaks up to give a laterally segregated film. We show that the growth of lateral inhomogeneities at the walls in turn causes the distortion of the interface in the transient wetting layer. By addressing the 1D phase equilibria of a polymer blend thin film confined between selectively attracting walls, we show that the breakup of a transient wetting layer is due to wall-blend interactions; there are multiple values of the volume fraction at the walls which solve equilibrium boundary conditions. This mechanism of lateral phase separation should be general.

DOI: 10.1103/PhysRevLett.111.125702 PACS numbers: 64.75.Va, 64.75.Cd, 64.75.St, 68.55.am

The ability to control the final morphology of polymer blend thin films is very important to the development of organic electronic devices such as organic or polymer light emitting diodes and photovoltaic films, since device morphology is linked heavily to performance. Lateral phase separation of polymer blend thin films is of particular interest, with several dynamical pathways having been identified, including initial phase separation at the surface of a spin-cast film which advances downwards as solvent is removed [1], and the initial formation of a transient wetting layer (bilayer) which subsequently breaks up [2]. The distinction between the layered morphology of vertical phase separation (one phase in contact with a surface) and the nonwet morphology of lateral phase separation (both phases in contact with a surface) was recognized in early numerical studies of binary blends [3]. The vertical layering of phases was realized both experimentally [4] and computationally [5,6], even in the nonwet regime [7,8]. Experiments later revealed that vertical layers can break up as lateral structures appear at a surface [9]. At present neither the dynamics of lateral phase separation nor the mechanisms driving the dynamics are well understood, in contrast to vertical phase separation. This Letter identifies and explains the dynamics of lateral phase separation via a transient wetting layer.

In this Letter, using simulations of a polymer blend film confined between selectively attracting walls, we show that, below the wetting temperature, the film first adopts a bilayer state, corresponding to a transient wetting layer, which then breaks up leading to a laterally segregated film. A more detailed analysis [10] shows that the phase equilibria of 2D polymer blend thin films are simply the 1D phase equilibria calculated in the dimension perpendicular to the confining walls only, the coexisting phases of the laterally segregated state existing under a chemical potential which cannot be predicted from a 1D consideration. With this in mind, we use simulation results and Hamiltonian phase portraits of the 1D phase equilibria [11,12] to demonstrate that wall-blend interactions control the dynamics of lateral phase separation via the breakup of a transient wetting layer.

A 1D description of an incompressible binary polymer blend (components A and B) confined between selectively attracting walls, using a Flory–Huggins–de Gennes free energy functional $\mathcal{F}$ supplemented with surface energy terms f that depend on the local volume fraction at the surface, is well established [13–16]. We denote the volume fraction of A by ϕ. Phase equilibria are the film profiles $\phi(z)$ with constant chemical potential μ, i.e.,

$$\frac{\delta \mathcal{F}[\phi(z)]}{\delta \phi(z)} = \mu, \tag{1}$$

which also satisfy a boundary condition at each confining wall, located at $z = 0$ and $z = d$. Using subscripts 0 and d to denote the walls, the boundary conditions are

$$+2\kappa(\phi_0)\nabla_z\phi|_0 = +\frac{\partial f_0}{\partial \phi_0} \equiv +h_0 + g_0\phi_0, \tag{2}$$

$$+2\kappa(\phi_d)\nabla_z\phi|_d = -\frac{\partial f_d}{\partial \phi_d} \equiv -h_d - g_d\phi_d, \tag{3}$$

where $h_{0,d}$ and $g_{0,d}$ are phenomenological parameters, ϕ_0 and ϕ_d are the volume fractions at $z = 0$ and $z = d$, respectively, and $\kappa(\phi) = a^2/36\phi(1-\phi)$. a is the underlying Flory-Huggins lattice spacing. Composition profiles existing independently (not in coexistence) must conserve the material/average blend ratio $\bar{\phi}$, which is enforced via correct choice of chemical potential (Lagrange multiplier) when solving for an equilibrium profile $\phi(z)$.

We performed 2D simulations of a symmetric polymer blend (average composition $\bar{\phi} = 1/2$) confined between selectively attracting walls. We obtained for our discretized diffusion equation

$$\frac{\partial \phi_{ij}}{\partial \tau} = \frac{1}{N}\nabla'^2\Bigg(\frac{\chi_C}{2|\chi-\chi_S|}\ln\frac{\phi_{ij}}{1-\phi_{ij}} - \frac{1-2\chi}{|\chi-\chi_S|}\phi_{ij} - \frac{(1-2\phi_{ij})}{\phi_{ij}(1-\phi_{ij})}\frac{\kappa_{ij}}{a^2}(\nabla'\phi_{ij})^2 - 2\frac{\kappa_{ij}}{a^2}\nabla'^2\phi_{ij} + \frac{\delta_{iD}\Delta z'^{-1}}{a|\chi-\chi_S|^{1/2}}\Big[\frac{\partial f_d}{\partial \phi_d} + 2\frac{|\chi-\chi_S|^{1/2}}{a}\kappa_{Dj}\nabla'_z\phi|_D\Big] + \frac{\delta_{i0}\Delta z'^{-1}}{a|\chi-\chi_S|^{1/2}}\Big[\frac{\partial f_0}{\partial \phi_0} - 2\frac{|\chi-\chi_S|^{1/2}}{a}\kappa_{0j}\nabla'_z\phi|_0\Big]\Bigg), \tag{4}$$

where i, j represent the coordinates (z, y), such that ϕ_{ij} is the volume fraction of component A at a given site ij. Δz is the mesh spacing (a square simulation mesh $\Delta y = \Delta z$ has been used), such that depth $d = D\Delta z$. We have used the contraction $\kappa_{ij} \equiv \kappa(\phi_{ij})$ and represented the Kronecker delta function by δ_{iS}: $\delta_{iS}(i = S) = 1$, $\delta_{iS}(i \neq S) = 0$ (the index S refers to the walls, i.e., $S = 0$ or $S = D$). In Eq. (4), periodic boundary conditions have been applied in the lateral dimension y, and we have normalized the surface energies by the mesh spacing Δz [17,18]. Space and time have been scaled by $z' = |\chi - \chi_S|^{1/2}z/a$ and $\tau = NM|\chi - \chi_S|^2 t/a^2$, respectively, where the mobility M is constant for simplicity, N is the degree of polymerization, and χ is the Flory-Huggins interaction parameter. χ_S and χ_C are the values of χ at the spinodal and critical points, respectively, hence, $\chi_S = \chi_C$ for a symmetric blend. Details of the derivation of our diffusion equation (4) and its numerical implementation will be given in a forthcoming publication [10].

For easy comparison with previous work [11], we use the following parameters: $N = 100$ ($\chi_C = 0.020$), $a = 1$, and $h_0 = -0.05$, $g_0 = 0.18$, $h_d = g_d = 0$ which corresponds to a B-attracting wall at $z = 0$ and a neutral wall at $z = d$. We discuss our results in terms of unscaled space z (in arbitrary units implied by a film depth calculation via the Hamiltonian method of Refs. [11,12]) and scaled time τ. Simulations were started with the film in an approximately homogeneous state $\phi(z, y) = 0.5 + \delta\phi(z, y)$, where $\delta\phi(z, y)$ was chosen randomly from a zero mean Gaussian distribution of width $\sigma = 0.05$.

Our simulations were performed below the wetting temperature ($\chi > \chi_W$). Snapshots of the simulations for depth $d = 20.1$ are given in Figs. 1 and 2 for $\chi = 0.026$ and $\chi = 0.022$, respectively, the subfigures proceeding forward in time from top to bottom (simulation animations are available online [19]). Figures 3 and 4 show 1D phase equilibria of depth 20.1, for $\chi = 0.026$ and $\chi = 0.022$, respectively, calculated using a Hamiltonian phase portrait method [11,12]. In Hamiltonian phase space, the (satisfied) boundary conditions Eqs. (2) and (3) are represented by straight lines. Phase portraits consist of the flow of coordinates (ϕ, $2\kappa\nabla\phi$) which minimize the bulk free energy functional $\mathcal{F}$ of the system. The solution trajectories are those parts of

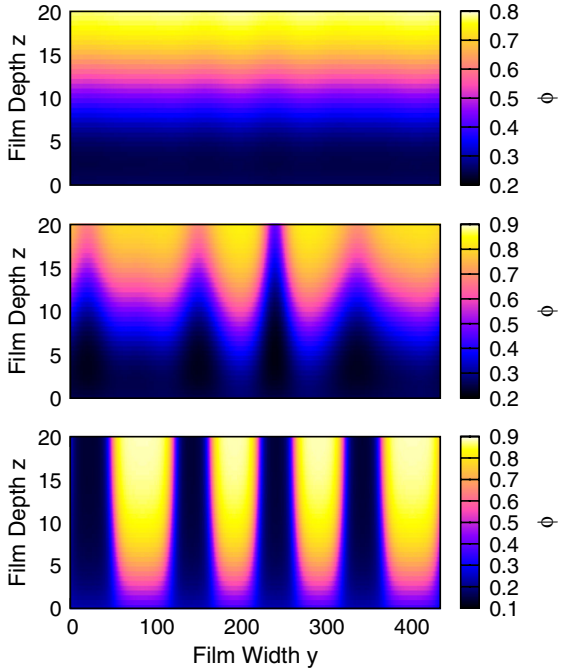

FIG. 1 (color online). $\chi = 0.026$ and $d = 20.1$, using $\Delta z = 0.50$ and $\Delta\tau = 1 \times 10^{-5}$. Top: metastable bilayer state ($\tau = 500$) with distortions in the interface corresponding to lateral inhomogeneities at the walls; Center: breakup of the interface in the bilayer state as a column of B-rich material reaches the $z = d$ wall ($\tau = 1665$); Bottom: stable laterally segregated state of coexisting phases ($\tau = 3655$). (Simulation animation available online [19].)

the phase portraits which flow between the wall boundary conditions. The phase portraits are altered by a Lagrange multiplier, in this case a chemical potential. Suitable choice of the Lagrange multiplier μ gives a trajectory for phase equilibria $\phi(z)$ with depth d and average composition $\bar{\phi}$. The phase portraits themselves provide significant insight, as the evolution of trajectories can be tracked graphically as depth, temperature, and wall interaction parameters change. In a forthcoming publication, we show that the calculated 1D phase equilibria precisely describe both the bilayer state and the laterally coexisting states from the simulations [10].

Figures 1 and 2 show that the film first develops a transient wetting layer corresponding to a B-rich (A-rich) phase coating the B-attracting (neutral) wall, respectively. Figures 3(a) and 4(a) show the trajectories of the lowest energy independently existing states, calculated using a chemical potential which assured material conservation $\bar{\phi} = 1/2$ in each case. The chemical potential obtained from simulations with no lateral inhomogeneities (no initial noise) and from 1D calculations of the equilibria are in perfect agreement [10], showing that this transient wetting layer is the bilayer corresponding to metastable equilibrium. This bilayer state is metastable with respect to a laterally segregated state [11]. In Figs. 1 and 2, there are

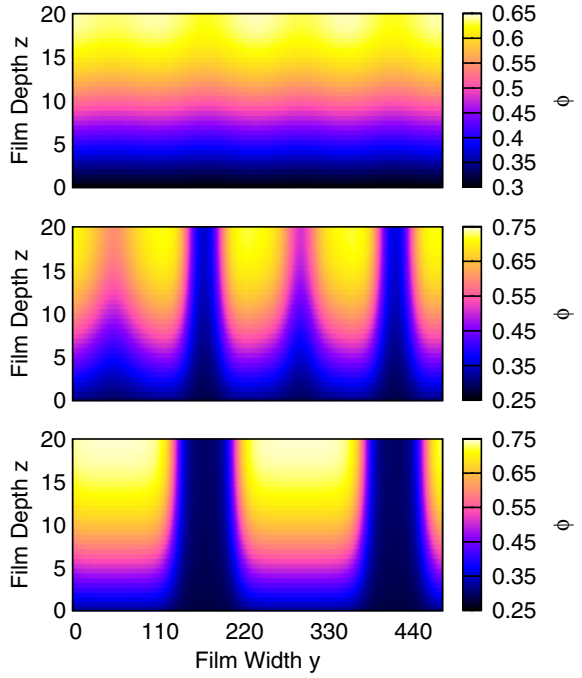

FIG. 2 (color online). $\chi = 0.022$ and $d = 20.1$, using $\Delta z = 0.56$ and $\Delta\tau = 0.25 \times 10^{-5}$. Top: late stages of metastable bilayer state with visible change of the volume fraction ϕ at the $z = d$ wall ($\tau = 1000$); Center: merging of adjacent A-rich lateral phases at around $y \approx 50$ and $y \approx 300$ to reduce interfacial energy ($\tau = 1800$); Bottom: stable laterally segregated state of coexisting phases ($\tau = 4756$). (Simulation animation available online [19].)

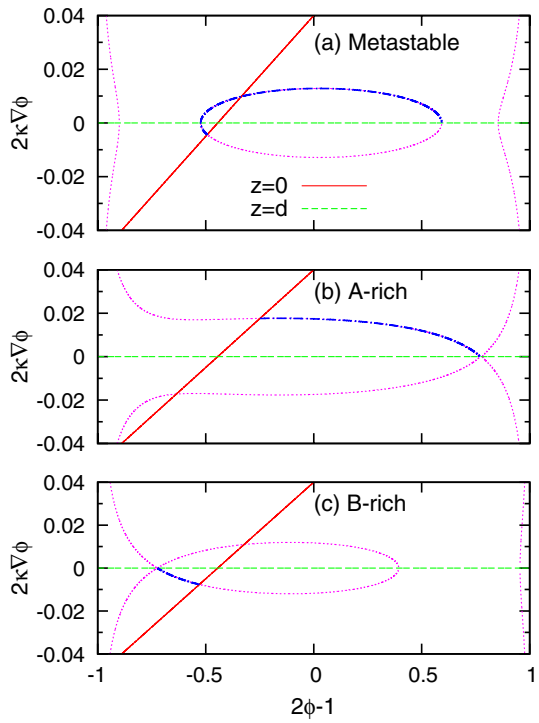

FIG. 3 (color online). 1D phase portraits for $\chi = 0.026$ and $d = 20.1$. The profile trajectories flow between the boundary conditions (BCs) set by the walls. (a) Metastable bilayer state ($\mu = -0.000\,119$); (b) A-rich lateral phase ($\mu = \mu_{\rm sim} = 0.000\,497$); (c) B-rich lateral phase ($\mu = \mu_{\rm sim} = 0.000\,497$). The crosses ϕ_d of all three flows with the $z = d$ BC are very different. The crosses ϕ_0 of the bilayer and B-rich flows with the $z = 0$ BC are quite similar, but distinct from the cross ϕ_0 of the A-rich flow.

small distortions of the interface in the bilayer arising from initial noise, but these distortions are invariably paired with lateral inhomogeneities at the walls.

Figures 1 and 2 also show that, as time proceeds, the interface in the bilayer becomes heavily distorted. Figure 1 shows a moment prior to interface breakup as a column of B-rich material reaches the neutral wall, and Fig. 2 shows merging lateral phases after the interface has broken up. We note that the average chemical potential remains nearly unchanged from that of the metastable bilayer state (with small distortions from initial noise) up until the interface begins to visibly break up. It can be seen that points where the interface touches down on the walls (Fig. 1) and points from where the lateral phases then develop (Fig. 2) are exactly the same points where the initial lateral variations at the walls took place. This strongly suggests that the inhomogeneities at the walls are responsible for the increasing distortion of the interface.

The bottom snapshots of Figs. 1 and 2 show the laterally segregated state corresponding to global equilibrium (the technicality that ''true'' global equilibrium corresponds to a single A-rich phase and a single B-rich phase is of little practical relevance). It is clear that the initial variations in ϕ at the walls have determined precisely where the lateral phases have formed. Parts (b)–(c) of Figs. 3 and 4 are trajectories for the lowest free energy laterally coexisting states. The chemical potential required for these calculations was obtained from the simulations when global equilibrium was reached. The resulting calculated 1D phase equilibria match the cores of the lateral phases from the simulation exactly [10]; hence, the 1D phase equilibria determine the behavior of the 2D system entirely, although a 1D approach does not yield the chemical potential required to sustain an interface between coexisting phases.

Since the phase equilibria resulting from simulations are in fact the 1D phase equilibria given in the phase portraits of Figs. 3 and 4, the mechanism of lateral phase separation via an instability in a transient wetting layer can now be seen in a new light. The bilayer state is unstable with respect to the laterally segregated state, since it has a higher free energy [11,12]. The dynamics of the breakup of the bilayer can now be addressed with reference to the phase portraits. The fact that distortions of the interface always correspond to variations in ϕ at the walls is nontrivial. Since the laterally coexisting phases formed where these variations at the walls began, and since the walls can, in fact, be the only mechanism driving interface distortion in the bilayer in our simulations, we argue that the breakup of the interface is a

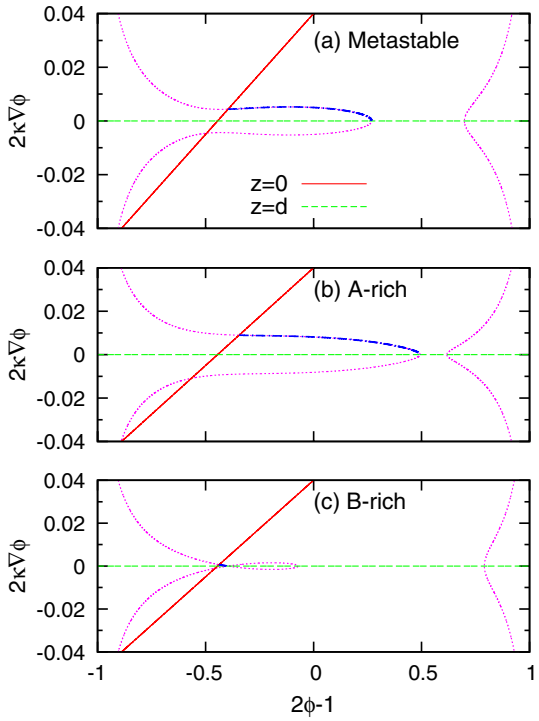

FIG. 4 (color online). 1D phase portraits for $\chi = 0.022$ and $d = 20.1$. The profile trajectories flow between the boundary conditions set by the walls. (a) Metastable bilayer state ($\mu = 0.000\,184$); (b) A-rich lateral phase ($\mu = \mu_{\text{sim}} = 0.000\,333$); (c) B-rich lateral phase ($\mu = \mu_{\text{sim}} = 0.000\,333$). The B-rich trajectory ($2\kappa\nabla\phi > 0$) lies very close to a fixed point. For all three flows, the crosses ϕ_d with the $z = d$ BC are rather different, but the crosses ϕ_0 with the $z = 0$ BC are quite similar.

result of wall-blend interactions, in particular additional solutions to the boundary conditions Eqs. (2) and (3).

For $\chi = 0.022$, Fig. 4 shows that the trajectory of the metastable bilayer passes through only one cross of the boundary conditions with the Hamiltonian flow for each confining wall, and the A-rich and B-rich phases of the laterally segregated state pass through these same crosses (we have verified, for $\chi = 0.023$, that the boundary conditions that metastable equilibria trajectories pass through do not necessarily determine which boundary conditions the coexisting equilibria can satisfy). As such, there is little variation of ϕ_0 compared to ϕ_d for the A-rich and B-rich solutions, which is why the $z = d$ wall contributes significantly more to the breakup of the interface in Fig. 2 than the $z = 0$ wall. The A-rich lateral phases appear to grow from the $z = d$ wall (the zero "bare" surface energy does not mean that the presence of a surface does not contribute to lateral phase separation dynamics).

For $\chi = 0.026$, Fig. 3 shows that the metastable solution passes through two solutions for Eqs. (2) and (3). ϕ_0 and ϕ_d of the A-rich and B-rich phases differ much more from their values for the metastable state than in the case of $\chi = 0.022$. This is especially true of ϕ_0 for the A-rich phase. Figure 1 shows that the breakup of the interface is due to significant variations in ϕ at both confining walls, the largest variations in ϕ_0 of the bilayer being precisely where the columns of A-rich phase form. This is expected from inspection of Fig. 3, which shows that ϕ_0 of the bilayer and B-rich phase are rather similar, but ϕ_0 of the A-rich phase is significantly different from both. Thus, the phase portraits offer practical insight into the dynamics of the breakup of the transient wetting layer.

Since our simulations did not include the presence of solvent, it is clear that solvent concentration gradients are not required for an instability of a transient wetting layer to exist below the wetting temperature. However, we suggest that solvent gradients caused by solvent evaporation may assist in several ways: (i) fast solvent evaporation provides lateral inhomogeneities in the transient wetting layer, which provide a kinetic route to the laterally segregated state that is often not reached (the breakup of the bilayer in our simulations and frozen out-of-equilibrium states found in experiments [20] show strong resemblances); (ii) the evaporation (and therefore reduction) of solvent at a surface allows phase separation to take place at that surface, via the same mechanism of wall-blend interactions presented here, which then proceeds into the film [21], the solvent in the bulk of the film providing increased miscibility and, therefore, preventing a bilayer from initially forming (the phase equilibria of a polymer-polymer-solvent film are of the same nature as those of a polymer-polymer film [22]); and (iii) overall reduction of solvent causes phase separation due to increased immiscibility of the blend and, therefore, phase separation occurs, the stages of which appear to proceed as in our simulations with high, medium, or low solvent concentrations corresponding to a bilayer, a bilayer with a distorted interface, or a laterally segregated state, respectively, [23].

Below the wetting temperature, the transient wetting layer which first forms, due to preferential attraction by the confining walls, breaks up because it is metastable with respect to a laterally segregated state. The transient wetting layer and laterally coexisting phases are in fact the lowest free energy 1D phase equilibria found in the dimension perpendicular to the confining walls. The intrinsic instability of the transient wetting layer (bilayer) is not to be confused with an instability of the interface between the vertically segregated phases of the bilayer. We conclude that wall-blend interactions drive the dynamics to the laterally segregated state by causing lateral inhomogeneities at the walls to grow, thereby distorting the interface in the bilayer until the bilayer breaks up into laterally coexisting phases. Ternary polymer-polymer-solvent blends should display the same mechanism.

[1] S. Ebbens, R. Hodgkinson, A. J. Parnell, A. Dunbar, S. J. Martin, P. D. Topham, N. Clarke, and J. R. Howse, ACS Nano **5**, 5124 (2011).

[2] S. Y. Heriot and R. A. L. Jones, Nat. Mater. **4**, 782 (2005).
[3] R. C. Ball and R. L. H. Essery, J. Phys. Condens. Matter **2**, 10303 (1990).
[4] R. A. L. Jones *et al.*, Europhys. Lett. **12**, 41 (1990).
[5] S. Puri and K. Binder, Phys. Rev. A **46**, R4487 (1992).
[6] G. Brown and A. Chakrabarti, Phys. Rev. A **46**, 4829 (1992).
[7] J. F. Marko, Phys. Rev. E **48**, 2861 (1993).
[8] S. Puri and K. Binder, Phys. Rev. E **49**, 5359 (1994).
[9] W. Straub, F. Bruder, R. Brenn, G. Krausch, H. Bielefeldt, A. Kirsch, O. Marti, J. Mlynek, and J. F. Marko, Europhys. Lett. **29**, 353 (1995).
[10] S. Coveney and N. Clarke (to be published).
[11] S. Coveney and N. Clarke, J. Chem. Phys. **137**, 174901 (2012).
[12] M. Souche and N. Clarke, J. Chem. Phys. **131**, 244903 (2009).
[13] P. G. de Gennes, J. Chem. Phys. **72**, 4756 (1980).
[14] J. W. Cahn, J. Chem. Phys. **66**, 3667 (1977).
[15] H. Nakanishi and P. Pincus, J. Chem. Phys. **79**, 997 (1983).
[16] I. Schmidt and K. Binder, J. Phys. (Paris) **46**, 1631 (1985).
[17] I. C. Henderson and N. Clarke, Macromol. Theory Simul. **14**, 435 (2005).
[18] J. I. Fukuda, M. Yoneya, and H. Yokoyama, Phys. Rev. E **73**, 066706 (2006).
[19] See Supplemental Material at http://link.aps.org/supplemental/10.1103/PhysRevLett.111.125702 for animations of the simulations used for Figures 1 and 2.
[20] S. Walheim, M. Böltau, J. Mlynek, G. Krausch, and U. Steiner, Macromolecules **30**, 4995 (1997).
[21] G. A. Buxton and N. Clarke, Europhys. Lett. **78**, 56006 (2007).
[22] M. Souche and N. Clarke, Macromolecules **43**, 5433 (2010).
[23] A. D. F. Dunbar, P. Mokarian-Tabari, A. J. Parnell, S. J. Martin, M. W. A. Skoda, and R. A. L. Jones, Eur. Phys. J. E **31**, 369 (2010).